Environ. Sci. Technol. **2000**, *34,* 2465−2471

Motion of Particles in Film Flow

SRINIVAS VEERAPANENI,*
JIAMIN WAN, AND TETSU K. TOKUNAGA
Earth Sciences Division, E. O. Lawrence Berkeley National Laboratory, Mail Stop 90-1116, Berkeley, California 94720

The effect of particle size (d_p) to film thickness (h_o) ratio on the motion of spherical particles in a stable liquid film flowing down an inclined flat surface is studied experimentally. Previously reported models that are based on force and torque balance are modified to predict the motion of particles that are smaller than film thickness. At low d_p/h_o values, particle velocity is observed to increase nearly linearly with particle size, reflecting the increasing influence of hydrodynamic drag as larger particles expose their surface to regions of higher fluid velocity. Good agreement between model predictions and experimental results is observed for small d_p/h_o ratios. When d_p/h_o is in the range of ∼0.7−1, particle velocities are observed to decrease rapidly with an increase in size. This may be attributed to the effect of the proximity of the free interface to the particle surface and also the deformation of the free surface induced by the moving particle. When d_p/h_o is in the approximate range of 1−1.75, particles ceased to move due to the surface tension acting on the particle along the circumference of the contact radius of the three-phase interface. For particles significantly larger than film thickness (d_p/h_o greater than about 1.7), particle velocity is observed to increase with its size as the particle motion is aided by the increased contribution from the gravitational force. For the range of film thicknesses and particle sizes studied, there appears to be a d_p/h_o range in which gravity force begins to dominate over surface tension force.

Introduction

The motion of particles in flowing films is important in many natural and engineered processes. For instance, several industrial processes such as antireflective coating of smooth glass surfaces involve depositing small particles on surfaces. Natural processes such as the transport of colloidal particles through partially saturated subsurface environments may facilitate the transport of contaminants sorbed onto them, or the particles can be contaminants themselves. A good understanding of the mechanisms responsible for colloid mobility in such environments is essential to predict and manage the spread of contaminants. A significant amount of work, both experimental and theoretical, has been reported over the past several decades to understand the mechanisms responsible for the transport of colloids in saturated porous media (*1*) and fractures. In recent years, there has been a growing interest in understanding colloid transport in partially saturated porous and fracture media. Colloids migrating downward through the vadose zone into groundwater may transport toxic chemicals. In the arid region of the Nevada Test Site, it has recently been reported that traces of plutonium migrated nearly 1.5 km through groundwater, possibly by sorption onto colloids suspended in water (*2*). Despite such indications of potential transport of colloidal contaminants, mechanistic understanding of colloid transport in partially saturated media is still lacking. Previous experimental investigations indicated that colloids are more efficiently retained when the porous medium is drier (*3*). In a series of investigations, Wan and co-workers (*4*−*7*) introduced a new mechanism of colloid sorption at gas−water interfaces under partially saturated conditions that may have significant effect on particle mobility. In a recent study (*3*), Wan and Tokunaga introduced the mechanism of "film straining", which hinders colloid mobility under unsaturated conditions. The premise of this hypothesis is that the gas−water interface can physically constrain colloid movement through regions of thin flowing liquid films that characterize fluid transport under unsaturated conditions. They introduced concepts of "critical matric potential" and "critical saturation", conditions at which direct connections between pendular rings are broken and film straining of colloids becomes dominant. Matric potential represents the saturation-dependent component of the chemical potential of water. The low and high extremes of matric potential indicate fully desaturated and fully saturated conditions of the porous medium, respectively. The effect of film straining on colloid removal was assumed to depend, rather intuitively, on the ratio of particle size and film thickness and on pore water velocity. Their model predicts that particle transport is inhibited if colloid size is larger than film thickness, while colloids smaller than film thickness are transported, even at saturations lower than the critical value. They tested their model against column experiments designed to study the transport of particles through unsaturated sands under a wide range of physical parameters such as particle and grain sizes, flow velocities, and degree of saturation. Thickness of water films adsorbed on the grains was estimated from matric potential, grain size, and gas−water surface tension using a modification of the Langmuir film equation. Good agreement between model predictions and experimental results was reported, using two adjustable parameters that relate particle removal by film straining to particle size to film thickness ratio and fluid velocity. However, the mechanistic understanding of the effect of the characteristics of films, particles, and medium surfaces on particle motion is still lacking. The relative importance of forces either facilitating (such as fluid drag and torque) or retarding (friction and surface tension) the motion of particles in flowing liquid films has not been previously investigated. To address some of these issues, this study was undertaken to investigate the effect of particle size/film thickness ratio on the motion of a spherical particle in a flowing liquid film. Due to the experimental difficulties associated with direct measurement of film thicknesses and particle movement at colloidal scale, experiments were conducted at larger scale. The present study on larger, noncolloidal particles focuses on hydrodynamic, surface tension, and body forces relevant even to colloids in thin films. However, due to the larger scales investigated, the influences of interfacial chemical interactions important in the colloidal limit are not examined.

Theoretical Considerations

Flow Field. The undisturbed flow field considered in the present study is that of an incompressible fluid film of thickness h_o flowing down a smooth surface inclined at an angle β from the horizontal. If the flow is assumed to be laminar, two-dimensional, and fully developed, the fluid

* Corresponding author phone: (510)495-2947; fax: (510)486-7797; e-mail: sveerapaneni@lbl.gov.

10.1021/es9912731 CCC: $19.00
Published on Web 04/29/2000

velocity and pressure are given by (for example, in refs *8* and *9*):

$$V_x(y) = \frac{g \sin \beta}{\nu}\left(h_o y - \frac{y^2}{2}\right) \quad (1a)$$

$$V_y = 0 \quad (1b)$$

$$P(y) = \rho_l g \cos \beta (h_o - y) \quad (1c)$$

where V_x is the velocity in the direction parallel to the solid plane, V_y is the velocity in the transverse direction, P is pressure, ρ_l is the density of the fluid, ν is the kinematic viscosity of the fluid, and y is the normal distance from the surface of the solid plane. The maximum velocity, $V_x|_{y=h_o}$, at the free interface, which is 1.5 times the average velocity, $V_{x_{ave}}$, is given by

$$V_x|_{y=h_o} = \frac{g h_o^{\,2}}{2\nu} \sin \beta = 1.5 V_{x_{ave}} \quad (2)$$

Three nondimensional numbers are usually employed to determine the nature and stability of the film flow:

$$\text{Reynolds number:} \quad Re = (V_{x_{ave}} h_o/\nu) \quad (3a)$$

$$\text{Froude number:} \quad Fr = V_{x_{ave}}/\sqrt{g h_o} \quad (3b)$$

$$\text{Weber number:} \quad We = V_{x_{ave}}^{\,2} \rho_l h_o/\sigma \quad (3c)$$

where σ is the surface tension of the liquid.

A transition in the nature of film flow from laminar to turbulent has been found to occur when *Re* is in range of 250−300 (*10*). The onset of gravity waves and capillary waves on the free interface is expected to occur for $Fr = 1-2$ and for *We* around 1, respectively (*10*). In all the experiments reported in this study, *Re* varied from 0.8 to 26, *Fr* varied from 0.2 to 1.4 and *We* varied from 10^{-4} to 0.14.

Particle Motion in Shear Flow. Particle motion in shear flow has been the subject of numerous investigations (*11*−*18*). However, most of these studies are limited by one or several of the following conditions: low Reynolds number flows, linear shear flows, small particles in slow poiseuille flows, and unbounded flows. None of these models are directly applicable to the flow field and the full range of particle sizes investigated in this work. However, some of the previous models may be applicable to the results obtained for small particles in this study. For small particles, the particle motion occurs within a short distance from the solid plane, where the fluid velocity is small and varies almost linearly with normal distance from the solid plane and the effect of free surface on the particle motion is negligible. For such a case, some of the models reported in the literature for the motion of particles in contact with a solid plane and in simple shear flows may be applicable as discussed in the next section.

The dominant forces acting on a particle submerged in a flowing liquid film and moving in contact with a smooth plane surface are fluid drag, lift, friction, buoyancy, and gravity. For a partially submerged particle, additional forces such as surface tension along the contact line between the film surface and the particle and pressure force also act on the particle, as shown in Figure 1. Given the scale of this study, short-range forces such as van der Waals and electrical double-layer interactions can be neglected. Such forces, when significant, can be included in eq 4.

Motion of a Completely Submerged Sphere with a Diameter Smaller Than Film Thickness. First, we consider the motion of a particle with a radius significantly smaller than the film thickness. Particle motion occurs within short distances from the solid plane, where the fluid velocity profile is almost linear (simple shear flow) and the particle motion may be assumed to be unaffected by the free interface. One can essentially consider the case of a motion of particle of radius, r_p, in contact with a plane wall in slow linear flow of shear rate γ (for example, see ref *13*). Under these assumptions, the dominant forces acting on the particle are fluid drag, lift, friction, buoyancy, and gravity and the torques associated with the fluid drag and friction forces. Balancing all the forces acting at the center of the particle and in the direction parallel to the solid plane and torques (about z-axis) acting on a completely submerged particle yields (*13*)

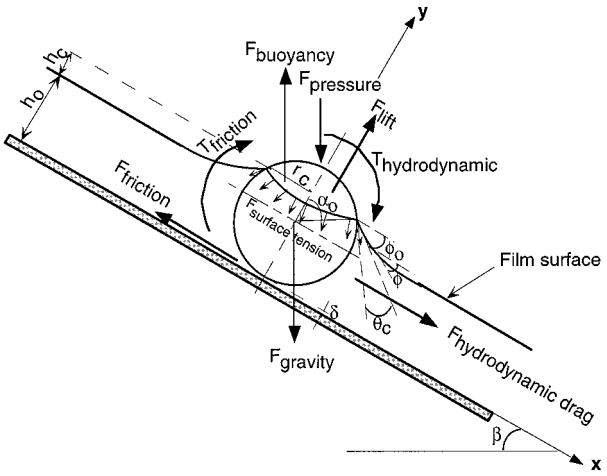

FIGURE 1. Forces and torques acting on a particle in a fluid film draining over an inclined plane.

$$F_{shear} + F_{trans} + F_{rot} + F_{gr} + F_{fric} = 6\pi\mu r_p(r_p\gamma F_s^*) + 6\pi\mu r_p(UF_t^*) + 6\pi\mu r_p(r_p\Omega F_r^*) + \frac{4}{3}\pi r_p^3 \Delta\rho g \sin\beta - \left(\frac{4}{3}\pi r_p^3 \Delta\rho g \cos\beta - F_{lift}\right)\mu_f = 0 \quad (4a)$$

$$T_{shear} + T_{trans} + T_{rot} + T_{gr} + T_{fric} = 8\pi\mu r_p^2(r_p\gamma T_s^*) + 8\pi\mu r_p^2(UT_t^*) + 8\pi\mu r_p^2(r_p\Omega T_r^*) + F_{fric} r_p = 0 \quad (4b)$$

where $\Delta\rho = \rho_s - \rho_l$, ρ_s is the density of the particle, ρ_l is the density of the fluid, μ_f is the dynamic coefficient of friction, μ is dynamic viscosity of the fluid, U and Ω are respectively the translational and rotational velocities of the particle, and F_{lift} is the lift force (see ref *13* for an expression to estimate F_{lift}).

The first three terms in eqs 4a and 4b represent the drag forces and torques acting on the sphere due to shear flow over a rigidly held sphere and due to two elementary motions of the sphere, viz., translation and rotation in a quiescent fluid and in the direction parallel to the bounding solid plane. The coefficients F_s^*, F_t^*, F_r^*, T_s^*, T_t^*, and T_r^* account for effect of the proximity of the solid boundary on the motion of the particle. These coefficients are calculated for a sphere in the proximity of a plane wall in linear shear under creeping flow conditions by several investigators (*13*, *19*, *20*) and are reported as a function of the gap between the sphere and the plane wall, essentially the average height of the roughness elements on the surface of the sphere (δ):

$$F_t^*, F_r^*, F_s^*, T_t^*, T_r^*, T_s^* = f(\epsilon) \quad (5)$$

where $\epsilon = \delta/r_p$. Values of these coefficients reported by King et al. (*13*) are used in this study.

Motion of a Sphere with a Diameter Comparable to But Smaller Than Film Thickness. When the particle size is

comparable to but smaller than the film thickness, it is expected that the proximity of the particle to the free interface will affect particle motion. The particle is also exposed to higher fluid velocities present in the regions closer to the free interface. The nonlinearity of the fluid velocity profile in this region also affects the motion of the particle. Under these conditions, development of an analytical solution for the motion of a particle is rather complicated. The complexity is further compounded by the possibility that the free interface may be deformed by the motion of the particle in its proximity, which in turn is likely to influence the motion of the particle. However, previous studies concerning the effect of the free interface on the motion of a particle under simplified conditions such as slow flow and semi-infinite domain may provide some guidance on the possible effects of free interface deformation on motion of particles with diameters comparable to but smaller than the film thickness and will be discussed later.

Motion of a Partially Submerged Sphere. For a partially submerged particle, the surface tension of the fluid results in deformation of the free interface around the particle. Solution for the motion of partially submerged particle requires finding the stress tensor by solving the Navier–Stokes equations and continuity equation with appropriate boundary conditions. This is an extremely difficult problem due to the three-dimensional nature of the problem and the presence of a moving free boundary, which requires a slip boundary condition in the neighborhood of the contact line (for example, see ref *21*). Analysis of the motion of the particle under these conditions is beyond the scope of the current study and has not been attempted. However, under some assumptions, the surface tension force and pressure force acting on a partially submerged particle can be estimated and is discussed below.

The component of the surface tension force normal to the solid plane acting on a partially submerged particle along the three-phase contact line (Figure 1) is given by

$$F_{\sigma_y} = 2\pi r_c \sigma \sin(\alpha_o - \theta_c) = 2\pi r_c \sigma \sin(\phi_o) \qquad (6)$$

where θ_c is the contact angle measured through the liquid phase, the angles α_o and ϕ_o are as indicated in Figure 1, and $2\pi r_c$ is the length of the contact line ($r_c = r_p \sin \alpha_o$).

The pressure force acting in the direction of gravity is given by

$$F_{\text{pressure}} = \pi r_c^2 \Delta P_c \qquad (7)$$

where ΔP_c is the excess pressure. Neglecting the density of air, $\Delta P_c = \rho_l g h_c$, with h_c being the capillary rise as shown in Figure 1.

Determination of the capillary rise h_c and the angle ϕ_o for a moving particle is quite complicated due to the presence of a moving free boundary, which requires a slip boundary condition in the neighborhood of the contact line. A rigorous hydrodynamic analysis addressing issues such as flow in the meniscus region and dynamic interface profile is needed. To simplify the problem and to obtain an approximation for the force due to surface tension acting on the particle, we can consider the case of quasi-static problem, wherein we assume the interface profile around the partially submerged particle to be the same as that of a particle in a stationary fluid film. The interface shape for such a physical condition can be obtained by solving the Young–Laplace equation. For an axi-symmetric meniscus, the Young–Laplace equation in cylindrical polar coordinates (r,z) is given by (*22*)

$$\sigma\left\{\left\{\frac{d^2z/dr^2}{[1+(dz/dr)^2]^{3/2}}\right\}+\left\{\frac{dz/dr}{r[1+(dz/dr)^2]^{1/2}}\right\}\right\} - g\rho_l z = 0 \qquad (8)$$

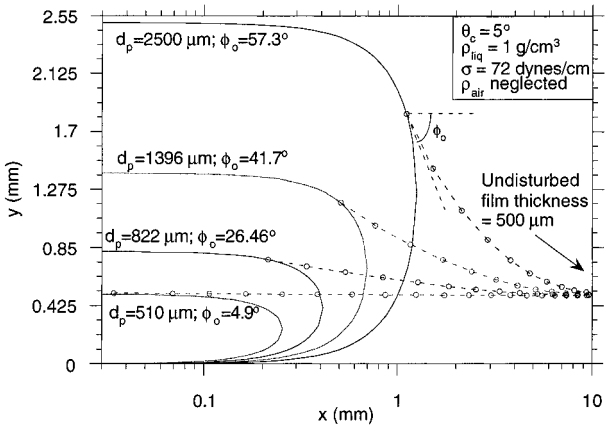

FIGURE 2. Interface profiles around spheres partially submerged in a film of 500 μm thickness, as calculated from the Young–Laplace equation. (Note that the shape of the spherical particle appears distorted due to the logarithmic scale on the *x*-axis.)

The boundary conditions on the meniscus profile are that the angle of the fluid interface with the particle surface is equal to the contact angle at the particle surface (eq 8a) and that the slope of the interface is zero at an infinite distance from the particle surface (eq 8b). The boundary condition that $z \to 0$ as $r \to \infty$ is already incorporated in eq 8:

$$dz/dr = -\tan(\phi_o) \text{ at } r = r_o \qquad (8a)$$

$$dz/dr \to 0 \text{ at } r \to \infty \qquad (8b)$$

Equation 8, along with the boundary conditions specified by eqs 8a and 8b, can be solved numerically to obtain the radius of the contact circle, inclination of the interface at the point of the contact, and capillary rise. The algorithm used to solve eq 8 numerically along with comparisons between observed and predicted interface profiles around particles partially submerged in stationary water films are discussed in Appendix A (see Supporting Information). To illustrate typical interface profiles around partially submerged particles, the calculated interface profiles around particles with diameters larger than a stationary film of thickness 500 μm are shown in Figure 2. The semilogarithmic scale is chosen to better illustrate the interface profile, even though it results in apparent distortion of the shape of the sphere. It is interesting to note that a thick meniscus surrounds the particle even when its diameter is about 3 times that of the film thickness. The surface tension force acting on these particles is proportional to the length of the three-phase contact circle ($2\pi r_c$) and is also dependent on the angle ϕ_o (see eq 6).

The variation of the parameters r_c and ϕ_o and surface tension acting on the particle (as estimated from eq 6) with the d_p/h_o ratio is shown in Figure 3. Contact angle measurements for small glass spheres in wetting fluids such as water or glycerol is a rather difficult task experimentally, as the contact angles for such systems are expected to be quite small. In Figure 3, r_c (solid line), angle ϕ_o (dotted line), and capillary rise including the film thickness ($h_o + h_c$, broken line) of the liquid around glass spheres partially submerged in a water film of thickness 500 μm are plotted as a function of their size, normalized with film thickness. To illustrate the effect of contact angle uncertainty, results for three values of contact angle are plotted. The interface profiles shown previously in Figure 2 are indicated on the *x*-axis at the appropriate particle size/film thickness ratios with solid circles. The contact circle radius and capillary rise are normalized with respect to particle size. The diameter of the particle is varied from 102 to 500% that of film thickness. The

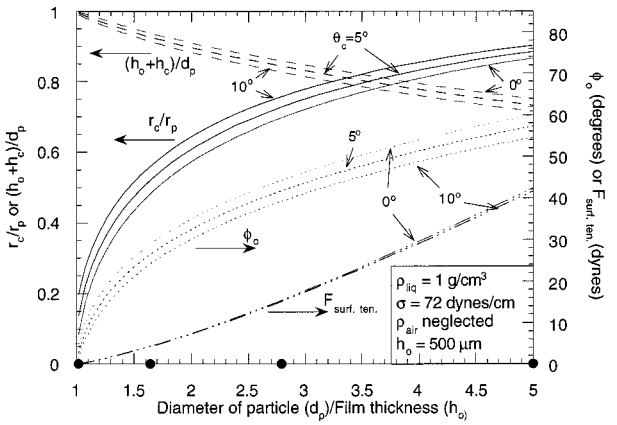

FIGURE 3. Contact circle radius, total capillary rise, interface angle at contact point, and surface tension as a function of diameter for partially submerged particle.

normalized contact circle radius (r_c/r_p) and the angle of the interface at the point of contact with horizontal (ϕ_o) increase with increase in particle size; a significant increase of these two parameters occurs when the particle diameter is 2−20% larger than the film thickness. The normalized capillary rise (including film thickness) decreases with particle size. The effect of contact angle, for the three values (0°, 5°, and 10°) shown in Figure 3, on these three parameters appears to be small. The surface tension force acting on the particle, calculated from eq 6 for two values of the contact angle, 0° and 10°, is shown in the figure (bottom lines). The effect of contact angle variation from 0° to 10° on surface tension estimation appears to be negligible. Note that the surface tension acting on the particle increases significantly with d_p/h_o.

After calculating the capillary rise as described above, the gravity force acting on a partially submerged particle can be estimated as follows:

$$F_{gr} = \frac{4}{3}\pi r_p^3 \rho_s g \sin\beta - \frac{1}{3}\pi(h_o + h_c)^2(3r_p - h_o - h_c)\rho_l g \sin\beta \quad (9)$$

Materials and Methods

The experimental effort in this study involved tracking the motion of spherical particles in a stable flowing film generated on an inclined plane surface. For practical ease, experiments were conducted at a scale considerably larger than that encountered in subsurface environments, with film thicknesses ranging from 120 to 670 μm and the particle sizes varying from 20 to 1000 μm. While acknowledging that the scale of this study may limit the direct applicability of the results from this study to subsurface environments, we believe that this study will help identify the dominant forces and torques acting on non-Brownian particles. A major drawback of the large scale of this study is the negligible importance of short-range forces due to van der Waals and electrical double-layer interactions. Such interactions may have significant influence on motion of colloids in subsurface environments.

A schematic of the setup is shown in Figure 4. A commercial glass plate of dimensions 100 cm × 50 cm was mounted on a 9 mm thick aluminum sheet. To minimize entrance and exit effects and to ensure that a steady film flow is established, the motion of the particles was tracked at the center of the glass plate within a viewing area of 4.3−13.5 mm^2. Edge effects were also assumed to be minimal as the large width of the glass plate ensured that the ratio of film thickness to channel width was less than 0.0014 for all

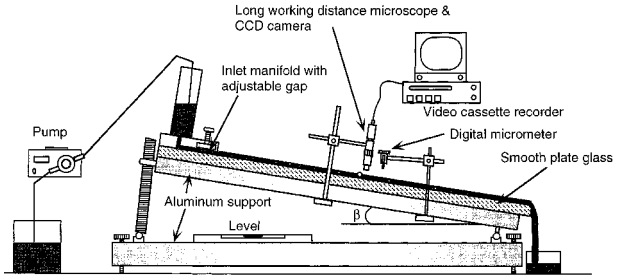

FIGURE 4. Schematic of the experimental setup.

the experiments. The large scale of the setup resulted primarily from an effort to reduce all edge and end effects. The channel was covered with plexiglass sheets to minimize disturbances due to room ventilation and to limit contamination. The inclination (β) of the aluminum sheet was adjustable over a range of 0−17°. The input manifold consisted of an acrylic cylinder attached to an aluminum block with a small opening. Fluid emerging from this opening flows through an adjustable narrow gap of 5 cm length and parallel to the longitudinal direction of the plate. Two types of pumps were used for different flow rates. A peristaltic pump with a pulse dampener was used for high flow rates, while a gear pump was employed for low flow rates. For films of thickness less than 200 μm, deionized water was used as feed solution. Glycerol solutions at concentrations ranging from 5 to 35 wt % were used to generate stable thick films. In some experiments, a surfactant (Triton X-100, Aldrich Chemical Co.) was used to vary the surface tension of the feed solution.

Film thickness was measured with a digital micrometer with a readability of ±0.001 mm. With the micrometer aligned normal to the glass plate, the head was moved downward slowly until it came in contact with the fluid film surface. Contact with the film surface was determined from visual observation, with the aid of a large magnifying lens. At the point of contact with the film surface, the micrometer was set to zero, and the downward movement of the micrometer was continued until it touched the glass surface. The reading at this instance was determined to be the film thickness. The procedure was repeated at least 15 times, and the average of all the readings was reported as the film thickness. This procedure was also repeated at the end of the experiment to check any variation in film thickness during an experiment. The variation between average film thicknesses measured before and after the experiment was found to be less than 2% in all the experiments and less than 1% in most experiments.

A long working distance microscope (Model K2, Infinity Photo-Optical Company) was used to observe the motion of particles through a small area at the center of the glass plate (in the longitudinal direction) and at a distance approximately 45 cm from the inlet. The viewable area varied from 1.8 mm × 2.4 mm to 2.7 mm × 5 mm depending on the objective and working distance. The movement of the particles was recorded using a monochrome charge-coupled device (CCD) camera (Cohu Inc.) attached to the microscope and a video cassette recorder (Model SVO-9500MD, Sony Corporation). The video cassette recorder has a horizontal resolution of more than 400 TV lines in S-VHS mode. Output from the CCD camera was also observed on-line using a monitor. At the end of each experiment, the images from the video cassette were digitized and downloaded, frame by frame, onto a computer using a frame grabber card. The images were analyzed using the public domain NIH Image program. The recorded image of an image analysis micrometer slide placed on the glass plate was used to calibrate the spatial dimensions of the video images. The distance traveled by

TABLE 1. Experimental Parameters

parameter	range
film thickness	122−672 μm
max film velocity at interface	1.04−13.3 cm/s
glycerol concn	0−35 wt %
liquid density	0.98−1.1 g/mL
liquid viscosity	0.01−0.027 g cm^{-1} s^{-1}
surface tension of liquid[a]	31.4−72.33 mN/m
inclination of plane	4.15−16.13°
particle diameter	20−1000 μm
particle density	2.2−2.5 g/mL
temperature	21−23 °C

[a] Varied using the surfactant Triton X-100 (Aldrich Chemical Co., Milwaukee, WI).

the particle was calculated by recording the position of the particle in consecutive frames of the recorded video. The velocity of the particle was calculated by dividing the distance traveled by time lapse between two frames. The diameters of the particles were also measured from the recorded images. Observation of the recorded images indicated that the particles were always in contact with the bottom glass surface.

The surface velocity of the fluid film was measured by introducing several types of floating hollow spherical particles as tracers and measuring their velocity. This method was similar to that used by Liu et al. (*23*). Five types of hollow spheres obtained from 3M Corporation were used: S22, borosilicate glass bubbles (density 0.22 g/mL and mode diameter 35 μm); SG, hollow silica particles with 5% crystalline silica (0.7 g/mL and 120 μm); Qcel, glass spheres with 15% boron oxide (0.21 g/mL and 50 μm); and two types of silica alumunina ceramic particles, W012 (0.7 g/mL and 60 μm) and W1600 (0.7 g/mL and 145 μm). Variation in the velocities of any particular type of tracer particles at different transverse positions within the viewing area of the microscope was observed to be quite small. The average velocities of these different tracer particles agreed well with each other. However, larger tracer particles (W1600) traveled at slightly lower velocities in thinner films. This can be attributed to the deformation of the film surface caused by these heavier particles. The surface velocity of the fluid film was assumed to be same as that of the tracer particles S22, which have the smallest diameter (average diameter = 35 μm) and relatively low density (0.22 g/mL).

Experimental Results and Discussion

The range of physical parameters investigated in this work are summarized in Table 1. Within these ranges, about 45 experiments were conducted, and on average 100 particles were analyzed in each experiment. In almost all the experiments, the trend of the data was observed to be the same. Results from two typical experiments are shown in Figure 5, panels a and b (experiments 10 and 45). The velocities of the particles, normalized with the maximum fluid velocity that occurs at the undisturbed free interface, are plotted as a function of particle size that is normalized with the film thickness. Four regions, as indicated in Figure 5a,b, can be identified.

In region I, the particle size is relatively small as compared to the film thickness, and the particle velocity is observed to increase with particle size. In this region, as the particle size increases, it is exposed to higher velocities as the fluid velocity increases linearly with distance from the solid plane at these depths. In addition, the presence of the free interface is not "felt" by the particle. The particle velocity in this region appears to be well predicted by the above-discussed model for the completely submerged particle for the following values of the two fitting parameters: $\epsilon = 0.03$ and $\mu_f = 0.15$. This

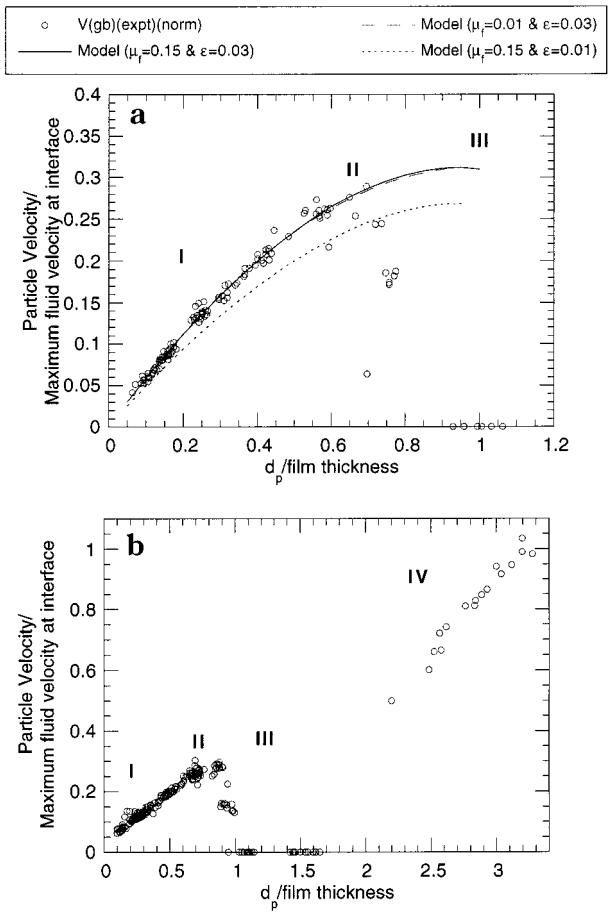

FIGURE 5. (a) Normalized particle velocity vs particle size (μ = 0.021 g cm^{-1} s^{-1}; ρ_l = 1.07 g/mL; h_o = 639.3 ± 11 μm; β = 8.36°; glycerol concentration 27.5 wt %). Note that the model is not valid for larger particle, whose motion is influenced by the free interface. (b) Normalized particle velocity vs particle size (μ = 0.014 g cm^{-1} s^{-1}; ρ_l = 1.022 g/mL; h_o = 253.5 ± 7.3 μm; β = 9.45°; glycerol concentration 9.98 wt %).

is expected since in this region the physical parameters satisfy the model assumptions such as slow flow and absence of the effect of the free interface. To illustrate the effect of the two fitting parameters, ϵ and μ_f, model predictions for two other sets of values for these two parameters are also shown in Figure 5a. For this region, model predictions appear to be relatively less sensitive to the coefficient of friction, μ_f, as indicated by the model predictions with $\mu_f = 0.15$ and $\epsilon = 0.03$ (Figure 5a). However, the roughness factor, ϵ, has more significant effect on the predicted velocities, as indicated by the curve with $\epsilon = 0.01$ and $\mu_f = 0.15$. The relatively high value for the particle roughness (3% of particle radius) needed to fit the model to the observed velocities can be thought of as a correction to the model, which assumes creeping flow. By increasing the roughness factor, we are essentially exposing the particle to higher velocities. Nevertheless, it is interesting to note that the model predictions and experimental results agree well in this region, even though all the assumptions of the model, such as creeping flow conditions, are not completely satisfied.

When the particle size is in the range 65−80% of the film thickness (region II), a significant decrease in particle velocities with increasing particle size is observed in most of the experiments. The above-described model does not predict this drop in velocity, as the possibility of the free interface deformation caused by the particle moving closer to the free surface and nonlinearity of the velocity profile is not explicitly accounted for in the model. As discussed earlier, we are not

aware of any previous investigations concerning the combined effect of a solid boundary as well as a free interface on the motion of a particle in a flow field characterized by a parabolic velocity profile. However, few investigators reported the effect of free interface deformation on the motion of a particle, under several simplifying assumptions. A series of theoretical studies reported by Lee et al. and Berdan et al. (*24*−*26*) dealt with the effect of the proximity of a free interface on the slow motion of a particle in an otherwise quiescent and unbounded fluid. They also assumed that the interface deformations are small. Under these assumptions, based on their theoretical analysis, they reported that the two elementary motions of the particle, rotation and translation in a direction parallel to the free interface, yield a force that is directed normal to and away from the interface (i.e., into the unbounded fluid). If we assume that qualitatively a similar force acts on the particle in the physical configuration of this work, this additional force will contribute to the friction force that is opposing the motion of the particle and might explain the decrease in the velocity of the particle. Under similar physical conditions, Danov et al. (*27*) investigated theoretically the flow caused by the motion of a sphere close to a viscous interface separating two fluids for a wide range of surface viscosities and different ratios of fluid viscosities. Their results indicated that, for an air−water interface, the torque coefficient on a particle rotating close to the interface (with no translation) of a quiescent fluid increases by as much as 50% when the distance between the sphere and the interface, normalized with particle radius, decreases from 1 to 0.01. However, they also reported that the drag coefficient of a translating particle (with no rotation) decreases by about 10% as the normalized distance of the particle from the interface decreases from 1 to 0.01. In another study, Fukuoka et al. (*28*) measured the drag and lift forces acting on a floating sphere that is restrained against rotation in a flowing glycerol solution. The distance of the sphere from the free interface at the top (or from the solid boundary below) was adjusted by filling the sphere with glycerin, water, or oil and thereby varying its weight. Their results indicated that the direction of the lift force changed when the sphere is closer to the free interface. Unfortunately, they did not specify the depth of the fluid but indicated that the lift force changed direction when the sphere center is in the neighborhood of 3.5 cm from the solid boundary beneath the particle and that the depth of the experimental flume (and not the depth of the flowing liquid) is 10 cm. They attributed the reversal in the direction of the lift force to the deformation of the free interface and reported that larger deformations caused higher negative lift forces. Results from this study also corroborate the decreasing velocities observed in region II of this study. Lift force, when acting away from the solid boundary, tends to alleviate forces that contribute to the friction force. A reversal in lift force direction due to the free surface deformation, as observed by Fukuoka et al., contributes to the frictional force, thereby inhibiting the motion of the particle. While the previous investigations of Lee et al., Berdan et al., Danov et al., and Fukuoka et al. provide a better understanding of the results we observed in region II, to obtain a quantitative estimate of the particle velocity one needs to evaluate the combined effect of the solid interface below the particle as well as the deformable free interface above the particle and the high velocities near the free interface on particle motion.

It should be mentioned that in a set of eight experiments, the drop in particle velocity in the size range of 65−80% of film thickness, as discussed above, is not observed. In these experiments, particle velocity is observed to decrease with particle size after reaching a maximum when the particle diameter is around 95% of film thickness. In all the other experiments, particle velocity dropped after reaching a maximum when the d_p/h_o ratio is in the range of 0.65−0.75. Reasons for this discrepancy are not known as all the experiments are conducted in a similar manner. It may be due to an untraceable variation in one or several experimental parameters such as film thickness measurement or image analysis. Several experiments that have been repeated after this set of experiments yielded results that are similar to those of earlier experiments as discussed above. With no other plausible explanation available at this time, we continue with our discussion of region III indicated in Figure 5a,b.

In region III, it is observed that particles with diameters even slightly greater than film thickness cease to move. It appears that even particles slightly smaller than the film thickness are stationary. However, given the uncertainties in film thickness and particle size measurements, it is possible that these particles may be slightly larger than the film thickness. The forces immobilizing the particles are the surface tension and pressure force acting on the particle in this region, as discussed earlier. As mentioned above, it is an extremely difficult task to do a complete force balance for a partially submerged particle moving in a flowing film. While forces such as surface tension, gravity, and pressure force acting on a partially submerged particle can be reasonably estimated, calculation of the drag force is intractable and is beyond the scope of this study. As illustrated in Figure 3, surface tension increases significantly with the size of partially submerged particles in a film of given thickness. For the experimental conditions yielding the data shown in Figure 5b, estimation of the normal component of the surface tension force based on eq 6 ($\theta_c = 5°$) acting on the particles with d_p/h_o values in the range of 1.1−1.7 yields values in the range of 0.23−2 dyn. This range of surface tension force results in additional friction force of 0.0345−0.3 dyn opposing particle motion with $\mu_f = 0.15$. As a crude approximation, we can compare this force with the drag force given by Stoke's law for particles in a free stream of velocity V. Note that, for the flow field in this work, the actual drag force is likely to be much lower than that estimated from Stoke's law due to the presence of the solid plane. Using Stoke's law, the drag force on particles with diameters in the range of 253−430 μm (corresponding to $1 < d_p/h_o < 1.7$) in a free stream of velocity V equal to the average velocity (2.5 cm/s) of the film for experimental conditions is calculated to be in the range of 0.006−0.01 dyn. Comparing the estimates of these two forces, we realize that the surface tension force dominates in this region.

In region IV (Figure 5b), when the particles are significantly larger than film thickness, the velocity of the particle is observed to increase almost linearly with the increase in size as the particle motion is aided by the increased contribution from the x-component of the gravitational force. However, the friction force also increases in this region as the contribution from the y-component of the gravitational force increases, although not as much as the x-component of the gravity force. It is interesting to note that there appears to be a particle size range in which gravity force begins to dominate over surface tension force. This is evident by the "dip" in the velocities of the particles between region III and region IV.

To study the effect of surface tension on movement of particles larger than film thickness, several experiments were conducted with solutions characterized by different surface tensions. The surface tension of the fluid was varied using a surfactant (Triton X-100, Aldrich Chemical Co., Milwaukee, WI). Other conditions such as film thickness and fluid velocity were kept constant (within the experimental variability). Results from two extreme cases, with no surfactant and with the concentration of surfactant close to but below critical micelle concentration, are shown in Figure 6. It is interesting to note that reducing the surface tension from 72 to 31 dyn/

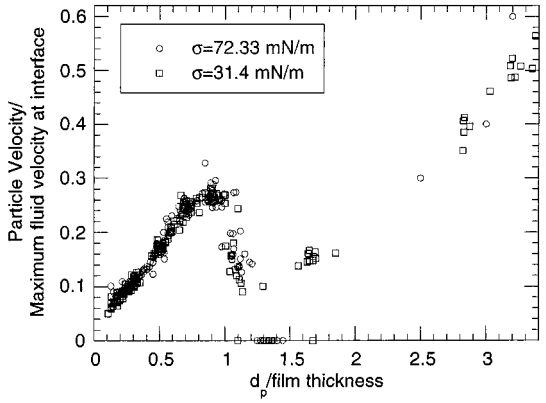

FIGURE 6. Effect of surface tension on particle velocity in film flow ($\mu = 0.0104$ g cm^{-1} s^{-1}; $\rho_l = 0.9982$ g/mL; $h_o = 229$ μm; $\beta = 9.98°$; surfactant used, Triton X-100).

cm did not have any effect on particle motion. For particles smaller than the film thickness, we do not expect any effect of surface tension variability. For such particles, as shown earlier, the interface has a negligible effect. However, when the particles are comparable to film thickness, we expected to see the effect of surface viscosities reported by Danov et al. (*29*). In their theoretical study, Danov et al. reported that the drag coefficient of particles moving in liquid films increases in the presence of surface active agents as compared to that of a particle in an unbounded liquid. However, the study of Danov et al. is limited to thin films and small Reynolds numbers, and the effect of surface active agents on particle motion reported by them may not be relevant to the current study due to its larger scale. Even for particles significantly larger than film thickness, the 56% reduction in surface tension appears to have negligible effect on particle motion. The surface tension force is significantly higher than most hydrodynamic forces, and to see any effect on particle motion, the surface tension needs to be lowered substantially, resulting in a higher value for *We*. Due to experimental limitations, we have not conducted any experiments at surface tension lower than 31 dyn/cm.

The experimental results from this study indicate that significant transport of non-Brownian particles can occur in film flows. When the diameter of the particles is significantly smaller than that of the film thickness, particle velocity is observed to increase almost linearly with particle size. When the particle size is comparable to film thickness, a siginificant drop in particle velocity is observed, possibly due to the effect of free interface. Surface tension appears to be the dominant force inhibiting motion of partially submeged particles with diameters comparable to film thickness. For partially submerged particles significantly larger than film thickness, gravity dominates motion of particles, and velocity is observed to increase with particle size. At colloidal scale, the interplay of hydrodynamic, surface tension, and body forces presented in this study is still relevant. However, the effect of short range forces such as van der Waals and double-layer interactions, which is negligible in the current study owing to its large scale, may be significant at smaller scales. Additional forces such as electrokinetic lift resulting from the relative sliding motion of a charged colloid past a charged fracture in an electrolyte solution may also become important. In addition, the effect of Brownian motion needs to be considered. We are currently extending our work to smaller scales and rough surfaces that are representative of colloid transport in the vadose zone.

Acknowledgments

This work has been supported by the Associate Director of the Office of Basic Energy Sciences, Division of Engineering and Geosciences, of the U.S. Department of Energy under Contract DE-AC03-76SF00098. We thank Drs. Stefan Finsterle and Hui-Hai Liu for their comments during the internal review process.

Supporting Information Available

Appendix A discussing the numerical method employed to solve the Young−Laplace equation, including equations, one figure, and references (6 pages). This material is available free of charge via the Internet at http://pubs.acs.org.

Literature Cited

(1) Tien, C. *Granular Filtration of Aerosals and Hydrosols*; Butterworth Publishers: Stoneham, MA, 1989.
(2) Kersting, A. B.; Efurd, D. W.; Finnegan, D. L.; Rokop, D. J.; Smith, D. K.; Thompson, J. L. *Nature* **1999**, *397*, 56−59.
(3) Wan, J.; Tokunaga, T. K. *Environ. Sci. Technol.* **1997**, *31*, 2413−2420.
(4) Wan, J.; Wilson, J. L. *Water Resour. Res.* **1994**, *30*, 11−23.
(5) Wan, J.; Wilson, J. L. *Water Resour. Res.* **1994**, *30*, 857−864.
(6) Wan, J.; Wilson, J. L.; Kieft, T. L. *Appl. Environ. Microbiol.* **1994**, *60*, 509−516.
(7) Wan, J.; Wilson, J. L. In *Transport and Remediation of Subsurface Contaminants*: *Colloidal, Interfacial, and Surfactant Phenomena*; Sabatini, D. A., Knox, R. C., Eds.; American Chemical Society: Washington, DC, 1994.
(8) Nusselt, W. *Z. Ver. Deut. Ing.* **1916**, *60*, 541−569.
(9) Bird, R. B.; Stewart, W. E.; Lightfoot, E. N. *Transport Phenomena*; John Wiley & Sons: New York, 1960.
(10) Fulford, G. D. *Adv. Chem. Eng.* **1964**, *5*, 151−236.
(11) Dandy, D. S.; Dwyer, H. A. *J. Fluid Mech.* **1990**, *216*, 381−410.
(12) Cherukat, P.; McLaughlin, J. B. *J. Fluid Mech.* **1994**, *263*, 1−18.
(13) King, M. R.; Leighton, J.; David, T. *Phys. Fluids* **1997**, *9*, 1248−1274.
(14) McLaughlin, J. B. *J. Fluid Mech.* **1993**, *246*, 249−265.
(15) Miyazaki, K.; Bedeaux, D.; Avalos, J. B. *J. Fluid Mech.* **1995**, *296*, 373−390.
(16) Bretherton, F. P. *J. Fluid Mech.* **1962**, *14*, 284−304.
(17) Brenner, H. *Chem. Eng. Sci.* **1964c**, *19*, 631−651.
(18) Saffman, P. G. *J. Fluid Mech.* **1965**, *22*, 385−400.
(19) Goldman, A. J.; Cox, R. G.; Brenner, H. *Chem. Eng. Sci.* **1967**, *22*, 653−600.
(20) Goldman, A. J.; Cox, R. G.; Brenner, H. *Chem. Eng. Sci.* **1967**, *22*, 637−651.
(21) O'Brien, S. B. G.; van der Brule, B. H. A. A. *J. Colloid Interface Sci.* **1991**, *144*, 210−221.
(22) Huh, C.; Scriven, L. E. *J. Colloid Interface Sci.* **1969**, *30*, 323−337.
(23) Liu, J.; Paul, J. D.; Gollub, J. P. *J. Fluid Mech.* **1993**, *250*, 69−101.
(24) Lee, S. H.; Chadwick; R. S.; Leal, L. G. *J. Fluid Mech.* **1979**, *93*, 705−726.
(25) Lee, S. H.; Leal, L. G. *J. Fluid Mech.* **1980**, *98*, 193−224.
(26) Berdan, C., II; Leal, L. G. *J. Colloid Interface Sci.* **1982**, *87*, 62−80.
(27) Danov, K. D.; Gurkov, T. D.; Raszillier, H.; Durst, F. *Chem. Eng. Sci.* **1998**, *53*, 3413−3434.
(28) Fukuoka, S.; Ishida, T.; E. Nigeme, E. *Trans. JSCE* **1978**, *10*, 130−132.
(29) Danov, K. D.; Aust, R.; Durst, F.; Lange, U. *Chem. Eng. Sci.* **1995**, *50*, 263−277.

Received for review November 11, 1999. Revised manuscript received March 17, 2000. Accepted March 20, 2000.

ES9912731